Atom probe microscopy of zinc isotopic enrichment in ZnO nanorods

C. N. Ironside, D. W. Saxey, W. D. A. Rickard, C. Gray, E. McGlynn, S. M. Reddy, and N. A. Marks

Citation: AIP Advances **7**, 025004 (2017); doi: 10.1063/1.4976299
View online: http://dx.doi.org/10.1063/1.4976299
View Table of Contents: http://aip.scitation.org/toc/adv/7/2
Published by the American Institute of Physics

Atom probe microscopy of zinc isotopic enrichment in ZnO nanorods

C. N. Ironside,[1,a] D. W. Saxey,[2] W. D. A. Rickard,[2] C. Gray,[3] E. McGlynn,[3] S. M. Reddy,[2,4] and N. A. Marks[1]
[1]*Department of Physics and Astronomy, Curtin University, Bentley, Perth, 6102 WA, Australia*
[2]*Geoscience Atom Probe, Advanced Resource Characterisation Facility, John De Laeter Centre, Curtin University, Building 301, Bentley, WA 6102, Australia*
[3]*School of Physical Sciences, National Centre for Plasma Science and Technology, Dublin City University, Glasnevin, Dublin 9, Ireland*
[4]*Department of Applied Geology, Curtin University, Bentley, WA 6102, Australia*

(Received 18 December 2016; accepted 30 January 2017; published online 8 February 2017)

We report on atomic probe microscopy (APM) of isotopically enriched ZnO nanorods that measures the spatial distribution of zinc isotopes in sections of ZnO nanorods for natural abundance ^{nat}ZnO and ^{64}Zn and ^{66}Zn enriched ZnO nanorods. The results demonstrate that APM can accurately quantify isotopic abundances within these nanoscale structures. Therefore the atom probe microscope is a useful tool for characterizing Zn isotopic heterostructures in ZnO. Isotopic heterostructures have been proposed for controlling thermal conductivity and also, combined with neutron transmutation doping, they could be key to a novel technology for producing p-n junctions in ZnO thin films and nanorods. [http://dx.doi.org/10.1063/1.4976299]

The study of isotopically enriched semiconductors has revealed novel physics because it provides a means of separating the contribution of the phonons and the electronic band structure to the physical properties of a material, including the optical, electrical and thermal properties.[1,2] ZnO has been extensively investigated,[3] partly because its large exciton binding energy offers the possibility of efficient light emitting devices if a p-doping technology can be reliably implemented. Furthermore, semiconductors containing zinc present a unique advantage, because isotopically enriched zinc is a by-product of the nuclear industry – in which depleted zinc is extensively employed in nuclear facilities,[4] and therefore Zn isotopes are readily available. The device possibilities of isotopically enriched ZnO include p-doping by nuclear transmutation doping (NTD).[5] After absorbing a neutron, ^{64}Zn transmutes to ^{65}Cu.[6] If the ^{65}Cu ion stays on the same lattice site as the ^{64}Zn ion from which it transmuted and forms a trap of the appropriate energy depth,[7] the ^{65}Cu could act as an acceptor dopant and help overcome the long-standing problem of reliably producing p-type ZnO.[8] However, in naturally abundant ^{nat}ZnO, 18% of the Zn is ^{68}Zn and when this isotope absorbs a neutron it is transmuted into Ga which could act as a donor impurity. So NTD of naturally abundant ZnO to produce p-type material is hampered by the production of donor impurities from the ^{68}Zn. To counteract this, NTD of ^{64}Zn isotopically enriched (^{68}Zn depleted) material could be used for p-type doping. Another device possibility includes engineering the thermal conductivity of ZnO nanorods by using an isotopic superlattice to reduce the thermal conductivity, whilst maintaining the electrical conductivity, and thereby improving the thermoelectric figure of merit.[9]

In this paper we outline a method for growing ^{64}Zn and ^{66}Zn isotopically enriched nanorods, and report on their characterisation via atom probe microscopy (APM), a technique which has been previously used to characterize ^{nat}ZnO nanorods[10,11] and isotopic heterostructures in Si and Ge.[12,13]

[a]Email: Charlie.Ironside@curtin.edu.au

Zn isotopically enriched ZnO nanorods have been previously grown for investigations of their optical properties and the growth method was reported.[14] The ZnO nanorods were grown on silicon (100) substrates, typically 1-4 cm^2 in size, and no attempt was made to remove the native oxide layer. The growth method involves a three step process.

In the first stage of the growth process, a seed layer was deposited on the substrate by drop-coating 3.75 μL of 0.005 M zinc acetate in absolute ethanol solution per cm^2 of sample area. This droplet was left for 20 seconds before being rinsed off the surface with copious amounts of ethanol. This process was repeated four more times for each sample. The substrates were then annealed at 350 °C in air for 30 minutes to decompose the zinc salt into zinc oxide. This process produces a thin layer of crystallographically aligned ZnO crystallites on the surface that act as nucleation sites for nanorod growth at later stages.

The second phase of the growth process is the deposition of a buffer layer of ZnO nanorods on the silicon substrate by CBD. A 0.02 M zinc nitrate solution was then slowly added to an equal volume of 0.8 M NaOH solution while stirring vigorously. The mixture was heated to approximately 70 °C and stirred gently. The sample was then submerged in the solution for 25 minutes while the temperature is maintained at 70 °C and the solution stirred gently. The sample was then removed, washed with copious amounts of deionized water and dried with a gentle nitrogen stream. This process leaves a layer of c-axis textured ZnO nanorods that acts as a buffer layer for subsequent growth of larger nanorods using vapor phase transport (VPT). Neither the seed nor buffer layers are isotopically enriched; they have the natural Zn isotope abundance.

The final stage in the growth of ZnO nanorods is carbothermal reduction VPT. 10 mg of ZnO powder and 10 mg of graphite powder were carefully mixed to produce a fine homogeneous powder mixture. This powder was then spread over a length of about 2 cm in an alumina boat. The silicon wafer was suspended above the powder with the ZnO buffer layer facing downwards towards the powder. The alumina boat was then placed into a quartz tube (inner diameter 37 mm) in a single temperature zone horizontal tube furnace. The quartz tube was purged with an Ar flow of 90 sccm for about 5-10 minutes. The temperature was then increased to 925 °C for 1 hour with the Ar flow remaining at 90 sccm. The furnace was then allowed to cool for several hours. When the temperature reached about 350 °C, the Ar flow was stopped and the alumina boat removed. This results in the growth of ZnO nanorods aligned with their c-axes normal to the substrate.

Isotopically enriched ZnO nanorod samples were grown by substituting the natural ZnO powder with Zn-enriched ZnO powders. The Zn isotopically enriched material used for growth in this study was enriched to 99.9% for ^{64}ZnO and 99.3% for ^{66}ZnO (obtained from Isoflex). The oxygen was in its natural isotopic abundance state (i.e. 99.76% ^{16}O).

For Atom Probe Microscopy (APM), nanorods have the advantage that they naturally form as the required, needle-like samples, and ^{nat}ZnO nanorods, with natural isotope abundances, have been previously been investigated via APM.[10,11,15] The process of collecting a nanorod from the wafer and mounting it on a silicon "microtip coupon"[16] is illustrated in Figure 1. The ZnO nanorod wafer was mounted in a Tescan Lyra 3, which has a focused ion beam combined with a scanning electron microscope (FIB-SEM). Figure 1(a) shows the dense 'forest' of ZnO nanorods grown vertically from the silicon wafer. A single nanorod is extracted, using electron beam Pt deposition to connect the top of the nanorod to a nanomanipulator and then using ion beam milling to release it from the substrate (Figure 1(b)). The stage is then lowered and moved so that the nanorod is directly above a post on a silicon microtip coupon. Ion beam Pt deposition is then used to connect the base of the nanorod to the post, and the top of the nanorod is then cut free from the nanomanipulator by ion beam milling (Figure 1(c), Figure 2). Finally, the ion beam is used with a 5kV accelerating voltage, in an annular milling pattern, to gently round-off the top of the nanorod for APM (Figure 2).

APM combines time-of-flight mass spectrometry and back-projection of field-evaporated ions from a specimen needle to achieve three-dimensional chemical and isotopic reconstructions at the atomic scale.[17,18] As such it is an excellent microscopy technique for the analysis of engineered nanostructures, and has been widely applied to the study of nanowires (or nanorods), and to the mapping of isotopic distributions within these and similar nano-scale heterostructures.[19,20] In this study, APM was utilized to quantify the level of isotopic enrichment in the ^{66}ZnO and ^{68}ZnO nanorods, and to look for

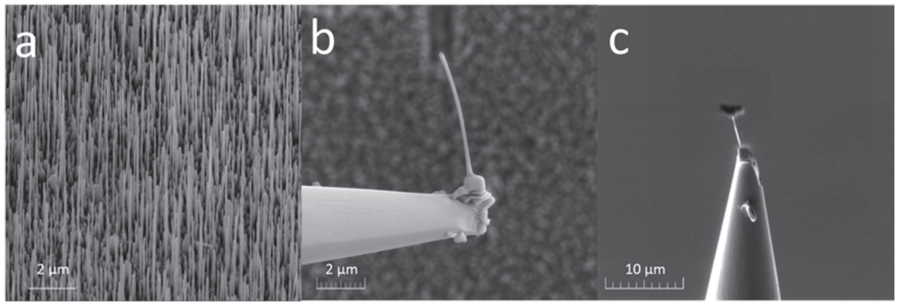

FIG. 1. (a) ZnO nanorod 'forest' grown on top of a silicon substrate. (b) A single nanorod attached to a nanomanipulator. (c) A single nanorod attached to the top of a silicon post of an atom probe microtip coupon.

isotopic variations that may be present along the length of the nanorod. In addition to the ^{66}ZnO and ^{68}ZnO specimens, ^{nat}ZnO nanorods grown from source material with natural isotope abundances were also analysed as a control, to experimentally determine the accuracy of APM isotopic measurements in this system.

Specimens were analysed in a CAMECA LEAP 4000X HR atom probe, at the Geoscience Atom Probe facility, Curtin University, Australia. This system uses pulses from a UV wavelength (355 nm) laser to initiate field-evaporation of ions from the apex of a needle-shaped specimen; an approach used previously in the study of ZnO nanostructures via APM.[11,15,21,22] Previous studies have noted several anomalies in the APM analysis of ZnO,[11,15,23] including: spatially non-uniform distributions of ions at the detector, varying with the laser energy; non-stoichiometric Zn:O ratios that are highly dependent on the conditions of the data acquisition and variable across the specimen surface; and variability in measured dopant concentrations with laser energy. When quantifying chemical variations or the overall composition of ZnO samples, these experimental artifacts are usually minimized through the use of low laser pulse energies, leading to high electric fields at the specimen apex.[11] However, for

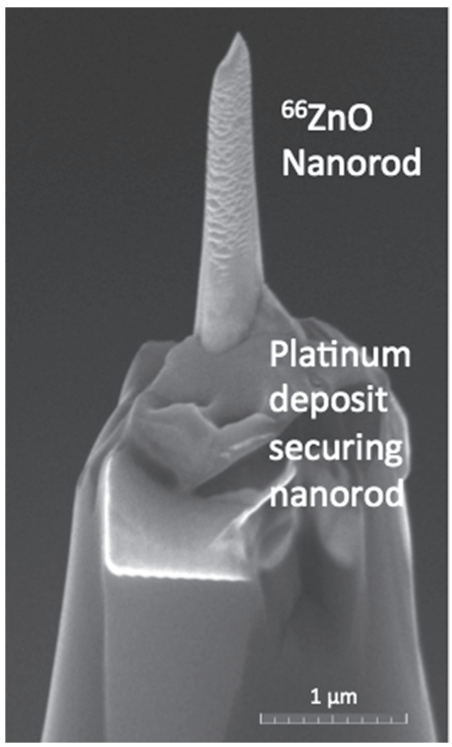

FIG. 2. Secondary electron (SE) image showing a ^{66}ZnO nanorod mounted on the microtip coupon.

isotopic studies, the situation is simplified, as none of the aforementioned effects are expected to depend strongly on the atomic mass, and no mass fractionation artifacts have been reported. Without the high-field constraint on the APM acquisition conditions, the ZnO nanorods could be analysed at higher laser energies (30–70 pJ per pulse), and therefore lower electric fields, allowing for greater specimen yields.

Two specimens were prepared from nanorods containing each isotopic abundance (natural abundance, ^{66}ZnO-enriched, and ^{68}ZnO-enriched), yielding at least one significant dataset in each case. The APM data were analysed using both CAMECA IVAS 3.6.14 and Igor Pro 7.0 software analysis tools, with the Zn^+ mass peaks carefully quantified in order to give an accurate measure of the isotopic abundances. To achieve an equivalent quantification for each isotopic peak, counts were summed within the same fixed range relative to each peak (Figure 3). Background noise and peak-overlap corrections were applied using curve fitting to estimate the local noise environment for each isotope peak.[17] Uncertainties were estimated from counting statistics associated with both the overall isotope mass peak, and with the estimated background noise and inter-peak overlaps. Potential mass peak interferences from ions such as Ni^+ (64 Da), Ba^{++} (66 and 68 Da), and ZnH^+ (67 and 68 Da) were considered insignificant based on the small magnitude, or absence, of peaks corresponding to other isotopes of Ni, Ba, and Zn.

The natural abundance Zn isotope fractions determined from APM analysis of the ^{nat}ZnO nanorod agree with well-established standard fractions[24] (Table I). This evidence attests to our APM methodology accurately measuring the Zn isotope fractions in both the natural and enriched nanorods. The ^{64}ZnO and ^{66}ZnO nanorods were found to be highly enriched in their selected isotopes, with enrichment factors of 7 and 26 respectively, when compared with the next most common un-enriched isotope, ^{68}Zn. The isotopic profile for ^{64}ZnO in Figure 3(a) shows significant variation over a distance of more than 100 nm along the nanorod axis. This data was collected from approximately 1 μm below the top of the nanorod due to a micro-fracture early in the APM acquisition. Earlier data from this specimen showed a concentration of 87.3% ^{64}Zn, and a correspondingly higher enrichment factor. By contrast, the enrichment of ^{66}Zn (Figure 3(b)) is notably constant over more than 100nm at the top of the ^{66}ZnO nanorod. Significantly, in each case the non-enriched isotopes were found to have natural abundance ratios with respect to each other, confirming that APM measurements provide a quantitative measure of isotopes within the enriched samples.

In this paper we have reported results on the Atom Probe Microscopy of ^{64}Zn- and ^{66}Zn-enriched, and on natural abundance, ZnO nanorods. The results from the natural abundance nanorods confirm

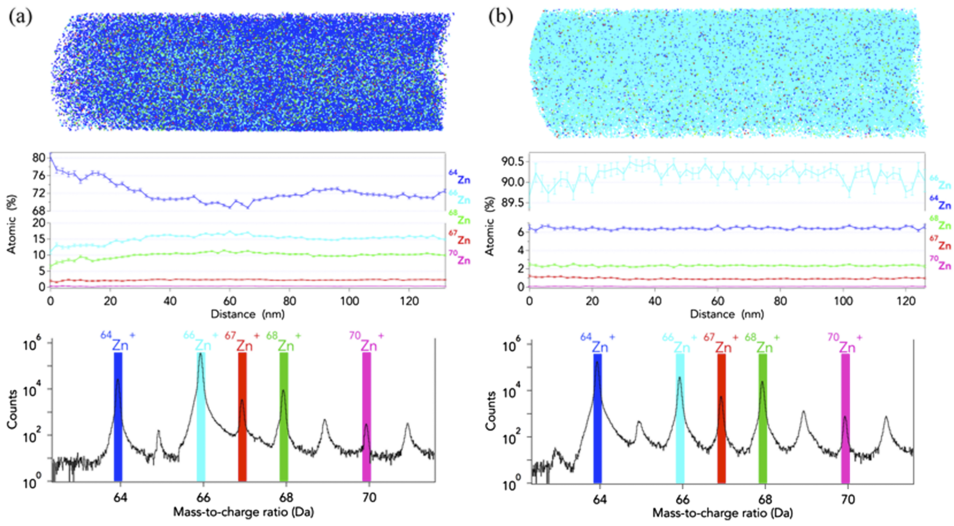

FIG. 3. APM atom maps (top) and corresponding isotopic profiles (centre) and mass spectra (bottom) for all stable zinc isotopes. Error bars in the isotopic profiles represent one standard deviation based on the atom counting statistics. The coloured bands in the mass spectra indicate the ranges over which the isotope counts were collected for each mass peak. (a) ^{64}ZnO nanorod sample. (b) ^{66}ZnO nanorod sample.

TABLE I. Zn stable isotope percentage in ZnO nanorod samples measured by APM; plus standard values for natural Zn isotope abundance. Uncertainties represent the expected standard deviation for each measurement.

Sample	^{64}Zn	^{66}Zn	^{67}Zn	^{68}Zn	^{70}Zn
^{nat}ZnO	49.28±0.02%	27.83±0.02%	4.20±0.01%	18.12±0.01%	0.562±0.003%
^{64}ZnO enriched	71.47±0.06%	15.60±0.03%	2.30±0.01%	10.30±0.02%	0.334±0.005%
^{66}ZnO enriched	6.44±0.02%	90.26±0.06%	0.88±0.01%	2.33±0.01%	0.078±0.002%
Natural abundance[24]	49.17±0.75%	27.73±0.98%	4.04±0.16%	18.45±0.63%	0.61±0.10%

that APM can measure zinc isotope ratios in ZnO nanorods with an accuracy of at least 1%. The precision of the technique is believed to be significantly higher, as indicated by the expected uncertainties in Table I. However, natural variations in Zn isotope abundances preclude these results from being used to derive any greater accuracy.

APM has also been shown to be a useful technique for measuring the spatial variation of the isotope distribution in the nanorod growth direction. In the ^{64}ZnO sample a variation in the ^{64}ZnO concentration of 10% over a distance of 60 nm was measured. However, this technique can also measure more abrupt variations, to within one monolayer, in isotope distribution.[25] Therefore APM is a suitable technique for characterizing nanostructures proposed by Haller[5] for nuclear transmutation doping to produce p-n junctions, and in the many other applications that have been suggested[2] for isotopically engineered materials, including thermoelectric devices.[26,27]

APM data sets were collected and analysed within the Geoscience Atom Probe laboratory, as part of the Advanced Resource Characterisation Facility (ARCF). The ARCF, under the auspices of the National Resource Sciences Precinct (NRSP)—a collaboration between CSIRO, Curtin University, and The University of Western Australia—is supported by the Science and Industry Endowment Fund.

[1] E. E. Haller, J. Appl. Phys. **77**, 2857 (1995).
[2] V. G. Plekhanov, *Isotopes in Condensed Matter* (Springer Berlin Heidelberg, Berlin, Heidelberg, 2013).
[3] Ü. Özgür, Y. I. Alivov, C. Liu, A. Teke, M. A. Reshchikov, S. Doğan, V. Avrutin, S.-J. Cho, and H. Morkoç, J. Appl. Phys. **98**, 041301 (2005).
[4] V. D. Borisevich, A. V. Pavlov, and I. A. Okhotina, Appl. Radiat. Isot. **67**, 1167 (2009).
[5] E. E. Haller, Semicond. Sci. Technol. **5**, 319 (1990).
[6] M. C. Recker, J. W. McClory, M. S. Holston, E. M. Golden, N. C. Giles, and L. E. Halliburton, J. Appl. Phys. **115**, 243706 (2014).
[7] M. Suja, S. B. Bashar, M. M. Morshed, and J. Liu, ACS Appl. Mater. Interfaces **7**, 8894 (2015).
[8] F. A. Selim, M. C. Tarun, D. E. Wall, L. A. Boatner, and M. D. McClusker, Appl. Phys. Lett. **101**, 029901 (2012).
[9] C.-H. Lee, G.-C. Yi, Y. M. Zuev, and P. Kim, Appl. Phys. Lett. **94**, 022106 (2009).
[10] N. Dawahre, G. Shen, S. Balci, W. Baughman, D. S. Wilbert, N. Harris, L. Butler, R. Martens, S. M. Kim, and P. Kung, J. Electron. Mater. **41**, 801 (2012).
[11] N. Amirifar, R. Lardé, E. Talbot, P. Pareige, L. Rigutti, L. Mancini, J. Houard, C. Castro, V. Sallet, E. Zehani, and others, J. Appl. Phys. **118**, 215703 (2015).
[12] Y. Shimizu, H. Takamizawa, Y. Kawamura, M. Uematsu, T. Toyama, K. Inoue, E. E. Haller, K. M. Itoh, and Y. Nagai, J. Appl. Phys. **113**, 026101 (2013).
[13] S. Mukherjee, U. Givan, S. Senz, A. Bergeron, S. Francoeur, M. de la Mata, J. Arbiol, T. Sekiguchi, K. M. Itoh, D. Isheim, D. N. Seidman, and O. Moutanabbir, Nano Lett. **15**, 3885 (2015).
[14] C. Gray, J. Cullen, C. Byrne, G. Hughes, I. Buyanova, W. Chen, M. O. Henry, and E. McGlynn, J. Cryst. Growth **429**, 6 (2015).
[15] J.-B. Seol, Y.-T. Kim, B.-H. Kim, and C.-G. Park, Met. Mater. Int **22**, 34 (2016).
[16] K. Thompson, D. J. Larson, and R. M. Ulfig, Microsc. Microanal **11** (2005).
[17] D. J. Larson, T. J. Prosa, R. M. Ulfig, B. P. Geiser, and T. F. Kelly, *Local Electrode Atom Probe Tomography* (Springer New York, New York, NY, 2013).
[18] T. F. Kelly and D. J. Larson, Annu. Rev. Mater. Res. **42**, 1 (2012).
[19] J. Qu, S. Ringer, and R. Zheng, Mater. Sci. Semicond. Process. **40**, 896 (2015).
[20] R. Agrawal, R. A. Bernal, D. Isheim, and H. D. Espinosa, J. Phys. Chem. C **115**, 17688 (2011).
[21] A. D. Giddings, Y. Wu, M. A. Verheijen, T. J. Prosa, F. Roozeboom, D. J. Larson, and W. M. M. Kessels, Microsc. Microanal. **20**, 526 (2014).
[22] S. Park, W. Jung, and C. Park, Met. Mater. Int. **19**, 1117 (2013).
[23] M. Karahka, Y. Xia, and H. J. Kreuzer, Appl. Phys. Lett. **107**, 062105 (2015).
[24] M. Berglund and M. E. Wieser, Pure Appl. Chem. **83** (2011).

[25] B. Gault, M. P. Moody, F. de Geuser, D. Haley, L. T. Stephenson, and S. P. Ringer, Appl. Phys. Lett. **95**, 034103 (2009).
[26] R. Frieling, S. Eon, D. Wolf, and H. Bracht, Phys. Status Solidi A **213**, 549 (2016).
[27] H. Bracht, S. Eon, R. Frieling, A. Plech, D. Issenmann, D. Wolf, J. Lundsgaard Hansen, A. Nylandsted Larsen, J. W. Ager III, and E. E. Haller, New J. Phys. **16**, 015021 (2014).